Journal of Materials Chemistry B

Pharmaceutical crystallization in surface-modified nanocellulose organogels

Journal:	*Journal of Materials Chemistry B*
Manuscript ID	TB-ART-06-2018-001554.R2
Article Type:	Paper
Date Submitted by the Author:	12-Sep-2018
Complete List of Authors:	Banerjee, Manali; Georgia Institute of Technology, Materials Science and Engineering Saraswatula, Sisira; Georgia Institute of Technology, Wallace H. Coulter Department of Biomedical Engineering Willows, Laura; Georgia Institute of Technology, Materials Science and Engineering Woods, Hannah; Georgia Institute of Technology, Materials Science and Engineering Brettmann, Blair; Georgia Institute of Technology, Materials Science and Engineering

Pharmaceutical crystallization in surface-modified nanocellulose organogels

Manali Banerjee[1], Sisira Saraswatula[2], Laura Grace Willows[1], Hannah Woods[1], Blair Brettmann[1]
[1] *School of Materials Science and Engineering, Georgia Institute of Technology*
[2] *Wallace H. Coulter Department of Biomedical Engineering, Georgia Institute of Technology*

Abstract
A significant research focus in the pharmaceutical industry is on methods to improve drug uptake into the body by increased dissolution of poorly-water soluble active pharmaceutical ingredients (APIs) or sustained drug release behavior, which results in higher overall uptake. Production of higher energy, higher solubility polymorphs is one approach to address this problem. Here, we utilize a natural material, cellulose nanocrystals (CNC), which has a high surface area covered with readily-modified hydroxyl groups, to form organogels that promote API crystallization into polymorphs that differ from as-received. We form the gels by oxidizing the CNCs and mixing them with an amine-containing surfactant, octadecylamine (ODA) in dimethylsulfoxide (DMSO) and we optimize the composition and preparation conditions for these gels. The APIs, sulfamethoxazole, sulfapyridine, and sulfamerazine, are added to the mixture prior to the gelation step and are expected to localize in the solvophobic regions of the physical gel and crystallize. We found that sulfamethoxazle recovered from the gels is in the amorphous state, while sulfapyridine crystallizes into a mixture of forms I, III and IV, and sulfamerazine crystallizes into forms I and II, which are different from the as-received materials. This system shows promise for rational design of nanocellulose organogel supports for heterogeneous crystallization of pharmaceutical materials with desired polymorphs.

Introduction

Oral dosage forms of pharmaceuticals, such as solid tablets, are preferred by patients, but provide challenges for developing advanced drug products. For many new active pharmaceutical ingredients (APIs), drug solubility in gastrointestinal fluids[1] is a major concern, as many newly discovered APIs fail in development due to poor water solubility.[2,3] One solution to this problem is a shift towards amorphous forms or crystalline polymorphs of the API with higher water solubility. Alternatively, use of forms of APIs with sustained release behavior is also promising, as this increases the duration for drug uptake into the body, while reducing the total required dosage of the drug.[4-7] Sustained release of APIs is also preferable to maintain constant drug concentration in the plasma and is often safer due to lower risk of precipitation.[7,8]

Amorphous pharmaceuticals have, in certain cases, shown higher bioavailability and improved solubility due to being a highly energetic solid state form of a material.[9] However, the amorphous form has poor stability and crystallizes over time, which has limited its use in industry.[10,11]

Current approaches to address amorphous stability focus primarily on mixing with polymers that interact strongly with the API[12] and processing approaches such as hot melt extrusion[13,14] and electrospinning[15,16] that improve the degree of mixing between the API and polymer.

Crystal engineering can also be used to improve drug release. Smaller crystals have a higher surface area and thus a faster dissolution rate[17] and less thermodynamically favorable crystalline polymorphs can have higher water solubility[18] or controlled drug release behavior, resulting in increased API absorption into the body.[19] Tailored crystallization of less thermodynamically favorable polymorphs is a challenge due to high sensitivity to conditions such as solvent, temperature, and cooling rate, which can lead to crystallization of unintended polymorphs.[20] In recent years, the desire for polymorph control has led to development of several new methods, with a shift toward heterogeneous crystallization, including crystallization in capillaries,[21] confinement in pores,[22,23] crystallization using polymers as seed crystals,[24,25] and crystallization from microgels.[26,27]

Heterogeneous crystallization provides a surface for nucleation, decreasing the effects of molecular conformations and the solvent, while providing a surface as a template.[25,28] New approaches involve heterogeneous crystallization onto surfaces that are not identical to the APIs, but have surfaces where the desired polymorph is more favorable than the most stable form.[24,29-32] This allows control over the domain size,[23,26,33] surface geometry,[34] and surface chemistry,[24,27,35] enabling polymorph selectivity. A type of heterogeneous crystallization, gel phase crystallization, presents a system with control over both surface geometry and surface chemistry,[27] making it a prominent avenue for rational design of heterogeneous nucleation of APIs. The small mesh size in the gels plays a dramatic role in enhancing nucleation kinetics, while the polymer-API interactions provide additional tuning at the optimal mesh size.[27,36-39] In this work, we use gels formed from nanocellulose, particles with a readily modified surface, as a platform (Figure 1). Using this microscale system, we can prepare a variety of functional surfaces to tune pharmaceutical crystallization.

Cellulose is an abundant natural biopolymer with high strength and stiffness.[40] Acid hydrolysis of plant fibers leads to a nanocrystalline form, cellulose nanocrystals (CNCs), which is highly ordered and has a low density and high aspect ratio. Readily accessible surface hydroxyl groups allow for easy modifications of CNCs, such as via carboxylation, silanization, acetylation etc.,[40] leading to many different available surface chemistries. A limitation to current commercially available CNCs is the inconsistencies due to their natural origins and methods of production. They are extracted from wood sources using harsh methods that vary by supplier, and it is a current thrust in the field to better understand and control the differences between suppliers and batches.[41] Due to this, we utilize CNCs to prepare organogels and modify the API polymorph, but do not at this time investigate the interplay between

spatial confinement and molecular interaction effects on crystallization, as was done for some of the prior studies on polymeric gels.[26,38,39]

Nanocellulose has shown the ability to form hydrogels through the formation of networks using very simple methods, such as increasing concentration in a suspension, hydrothermal treatment, and sonication.[42-44] These hydrogels and their derivatives, including membranes, films, and aerogels, have shown promise for uses in the biomedical field such as cell encapsulation and controlled release of drugs.[45-48] Due to the surface tunability of CNCs, network formation can also be induced using solvophobic surface modifications, resulting in organogels that can be used for the crystallization and production of APIs.[49]

In this work, we optimize network formation in a water-free nanocellulose gel system to create a stable support for drug nucleation (Figure 1). By changing the surface chemistry of CNCs using a 2-step process, carboxylation followed by physical adsorption of the long-chain octadecylamine (ODA), a physical network was formed with a large solvophobic area available for molecular interactions with poorly soluble APIs. This approach was reported previously by Ruiz-Palomero et al., who prepared nanocellulose organogels and crystallized multiple APIs.[49] We take this work further in examining the effect of composition and preparation methods on gel strength, providing more in-depth focus on three APIs and examining the dissolution properties of the resulting dried gels containing recrystallized APIs. We demonstrate the utility of the nanocellulose gels for polymorph selection using a series of three sulfonamide antibiotics: sulfamethoxazole, sulfapyridine and sulfamerazine. These drugs have low solubilities in water and exist in many polymorphic and solvate forms[32,50,51] and are thus excellent model drugs for the design of a polymorph-selective crystal engineering system. The optimized nanocellulose gels provide a favorable environment for API solidification into less stable forms, including the amorphous form (sulfamethoxazole) and different polymorphs than as-received (sulfapyridine and sulfamerazine). These highly tunable gel supports offer a promising approach for rational design of materials for controlling the solid form of the APIs.

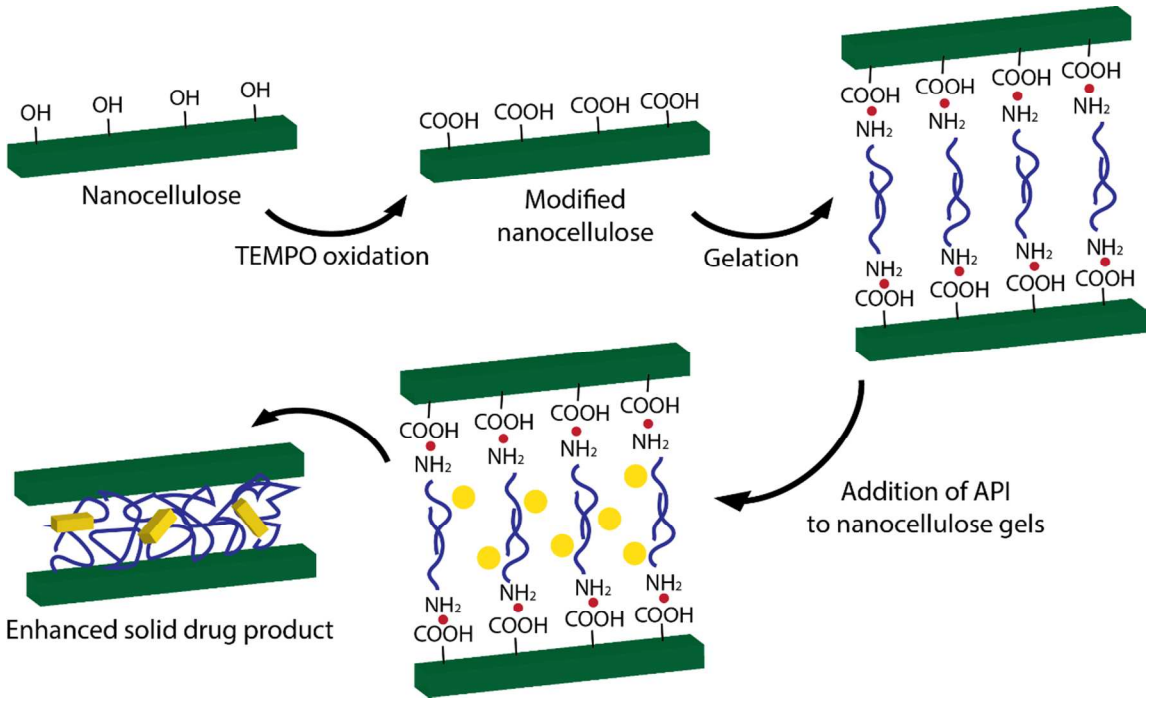

Figure 1: Schematic representation of surface modified nanocellulose organogels used for pharmaceutical crystallization.

Experimental

Materials:

CNCs were produced by the Forest Product Laboratory (Lot # 2014-FPL-CNC-064) and distributed by the University of Maine Process Development Center. The CNCs were obtained as a 11.8% slurry and were freeze-dried prior to use. 2,2,6,6-Tetramethyl-1-piperidinyloxyl free radical (TEMPO) and sulfapyridine (SP) were obtained from TCI. Sulfamethoxazole (SMX) was obtained from MP Biomedicals. ODA, sodium bromide (NaBr), sulfamerazine (SMZ), sodium hypochlorite (NaOCl), and polyethylene imine (PEI) were all obtained from Alfa Aesar. 1,8-diaminooctane and ethanol were obtained from Acros Organics. Dimethyl sulfoxide (DMSO) was obtained from Fisher Chemical. All of these were used as received.

Surface modification – TEMPO mediated oxidation:

Oxidation of CNCs was done using the procedure by Habibi *et al*.[52] Briefly, about 1 g of freeze dried CNCs were suspended in 150 mL water and stirred for 15 min. TEMPO (0.035 mol/mol CNC) and NaBr (0.5 mol/mol CNC) were added and the suspension was further stirred for 15 min. NaOCl (0.2-6 mol/mol CNC) containing 11-15% active chlorine was added in a dropwise manner to start the oxidation

procedure. The pH of the mixture was kept between 10.5 and 11.5 with the addition of 0.5 M NaOH. The oxidation was deemed complete once the pH of the mixture stopped decreasing and the reaction was terminated by adding 5 mL ethanol. Finally, the oxidized nanocellulose (O-CNC) was freeze-dried to obtain a white powder.

The degree of oxidation of the O-CNC was qualitatively observed using Fourier transform infrared spectroscopy (FTIR). Prior to oxidation there were no peaks between 1600-1700 cm^{-1} and post oxidation a peak appeared at around 1610 cm^{-1}, attributed to the salt form of carboxylated CNC.[53] The degree of oxidation was quantitatively measured using conductimetric titrations. Approximately 50 mg of the freeze-dried O-CNC was suspended in 50 mL water and stirred. 2 mL of 0.1 M HCl was added to the suspension to obtain the carboxylic acid form of O-CNC. This was titrated against 0.1 M NaOH and the following equation was used to calculate the amount of carboxyl group, which corresponds to the degree of oxidation:[54]

$$DO = \frac{162 \times C \times (V_2 - V_1)}{w - 36 \times C \times (V_2 - V_1)}$$

Where C is the concentration of NaOH, w is the mass of O-CNC used, and (V_2-V_1) is the volume of the flat plateau region of the conductivity curve (which corresponds to the amount of base required to neutralize the weak carboxyl groups present on the O-CNC).

Gelation:

The gelation was performed by mixing prescribed amounts of O-CNC and ODA with DMSO, vortexing for 30 sec and sonicating in a bath at room temperature for 10 min. The mixtures were then heated to 70□ to disrupt intermolecular interactions and then cooled to initiate gelation. A variety of different mixing and cooling conditions were used to optimize the gelation and all samples are listed in supplementary information Table S1.

Incorporation of pharmaceuticals:

The APIs (concentrations ranging from 50-500 mg/mL) were added to the mixture in the network formation step after the ODA and O-CNC had been properly dissolved and dispersed into DMSO. The mixtures were then heated and cooled similarly to the gels without APIs in them. This procedure was followed for each of the three APIs, SMX, SP, and SMZ.

To run certain characterization tests, the samples (with and without APIs) were dried overnight at 60□ under vacuum. The recrystallized pharmaceuticals were obtained as a mixture of dried powders (O-CNC, ODA, and API).

Characterization of gel strength:

Gelation was confirmed using an inversion test, where samples are turned upside-down and observed. They are considered to be gels if they remain intact after inversion and considered to be liquids if they flow under their own weight.[55] To characterize the strength of the gels, they were inverted and shaken at 400 RPM using a Thermo Fisher Max Q shaker. The time required for them to de-gel and flow was measured and used as a quantitative indication of the strength of the gel.

Rheological studies were also performed to assess the strength of the gels. A TA Instruments Discovery 3 Hybrid rheometer was used with a 40 mm diameter plate and a 2° cone. 2 mL of each gel was analyzed at a gap of 53 μm at 25□. Stress sweep experiments were performed at a frequency of 1 Hz with the stress ranging from 0.1 to 1000 Pa.

Pharmaceutical characterization

Differential scanning calorimetry (DSC) was performed on a Mettler Toledo DSC 3+. Samples were heated at 10□/min from 40-350□. DSC was used to determine thermal behaviors of the samples including melting points and phase transformations. As-received materials were also tested for reference.

X-ray diffraction (XRD) was performed using a Panalytical XPert Pro Alpha-1 XRD operated at 40 mA. The range of scanned angles was 1^o to 40^o using a $1/16^o$ anti-scatter slit and a 0.04 radian soller slit. These scans were done on the dried samples to determine the crystal structure of the recovered APIs. As-received materials were also tested for reference.

Optical microscope images of the APIs were taken using a LEICA DMi8 microscope in transmission mode.

Drug dissolution studies were performed to determine the drug release kinetics. Samples containing 8.3 mg API were added to 100 mL of 0.01M HCl. Aliquots were taken at specific time intervals ranging from 2 minutes to 48 hours. These aliquots were analyzed using a Beckman Coulter DU 800 UV-Vis Spectrophotometer between 200 and 400 nm. The wavelength of absorption for each drug and calibration curve was determined using standards ranging from 0.006 mg/mL to 0.03 mg/mL. The dissolution measurements were taken at the wavelength of highest absorption for each API (265 nm for SMX, 240 nm for SP, and 255 nm for SMZ).

Physical mixtures were made by combining 30 mg of O-CNC, 90 mg of ODA, and 600 mg of each API. This was done to determine whether the gelation and gel-phase crystallization produced APIs with different dissolution behavior than a physical mixture of the same components. These mixtures were ground together with a mortar and pestle before performing the same dissolution studies as above.

Results

Nanocellulose Gels

CNCs were modified using TEMPO oxidation to produce a surface containing carboxyl groups (O-CNC). In this study, these were the terminal surface modifications, however further functionalization is straightforward with this base surface to work from. Oxidation of the CNCs can be confirmed qualitatively using FTIR. Figure 2-A demonstrates the appearance of a strong C=O peak after oxidation at 1600 cm^{-1}. This corresponds to the carboxyl group on the O-CNC in its sodium salt form. As the molar ratio of the oxidant (NaOCl) to the CNC is increased, there is an increase in the degree of oxidation, seen as an increase in the peak height at 1600 cm^{-1} as the ratio is increased

from 0.2 moles of NaOCl per mole of CNC (blue) to 5 moles of NaOCl per mole of CNC (brown). The degree of oxidation can also be measured quantitatively using conductimetric titrations. The degree of oxidation depends on the molar ratio of the oxidant used and, for CNCs, reaches a maximum at approximately 30% conversion of –OH to –COOH groups (Figure 2-B). This limit arises from the accessibility of the OH groups in the CNCs, as only hydroxyls at the surface (as opposed to inside the crystal bulk) can be modified by the oxidation reaction.[52]

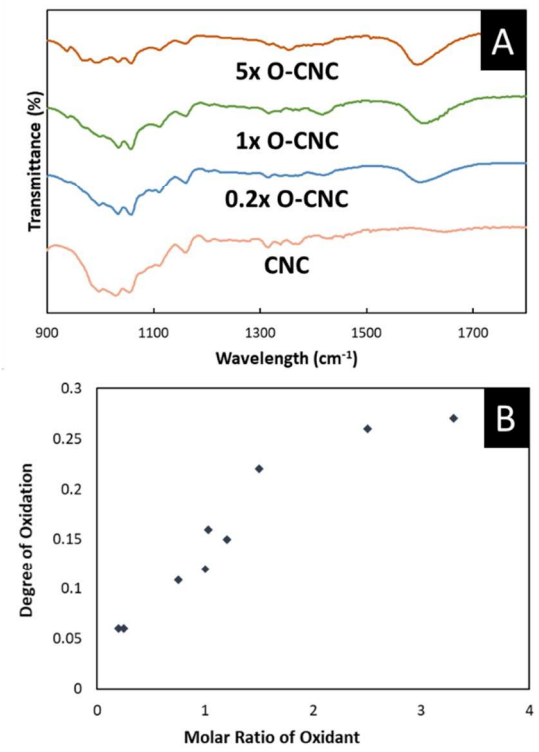

Figure 2: Oxidation of nanocellulose characterized via FTIR and conductimetric titrations. A: FTIR shows the appearance of the C=O peak at 1600 cm^{-1}, which increases with molar ratio of oxidant to CNC. B:

Conductimetric titrations show that the degree of oxidation plateaus around 30%

Prior to preparing organogels containing APIs, we identified the conditions under which nanocellulose organogels form and how the mixing procedures and mixture components influence gel formation and stability. Two gel preparation parameters were tested, the order of mixing and the cooling method, and three different mixture component contributions were examined, the ratio of ODA to O-CNC, the concentration of O-CNC and the degree of oxidation of O-CNC. All five were found to impact the formation of the gels and the gel strength, and an optimal procedure and mixture were identified for use with APIs.

At low concentrations of O-CNC (3 mg/mL) and ODA (5 mg/mL), the mixtures did not pass the inversion test and, though they appeared gelled at 4□, the mixture turned into a liquid once it was returned to room temperature. Visible gels formed once the O-CNC concentration reached 5 mg/mL and ODA concentrations were at 10 mg/mL. However, gelation was only possible once the concentration of ODA was more than twice that of O-CNC (Figure 3-B, C, D, and E versus 3-A). We examined the influence of the ratio of O-CNC to ODA across many O-CNC concentrations and found that, at a 1:1 ratio of O-CNC to ODA, no gelation was observed regardless of the concentration of each component. However, once the ODA concentration is at least double that of O-CNC, gelation was observed at as low as 5 mg/mL O-CNC. The gels continue to form as ODA is added beyond the 2:1 ratio (increasing the ratio of ODA to O-CNC), but

decreases again once the concentration of ODA in the mixture exceeds the solubility of ODA in DMSO (32 mg/mL), thus a 3:1 ODA:O-CNC ratio was selected as an optimal ratio for studies with the APIs.

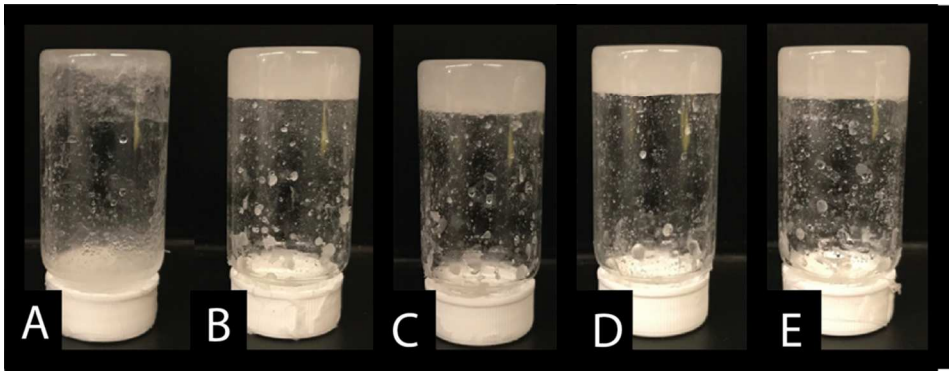

Figure 3: Nanocellulose organogels with 10 mg/mL O-CNC and increasing concentrations of ODA (a. 10 mg/mL, b. 20 mg/mL, c. 30 mg/mL, d. 40 mg/mL, e. 50 mg/mL)

An initial observation of the gel strength can be performed using simple shaking tests, where the strength of the gel is correlated to the de-gelling under disruptive forces. The gels are shaken at 450 RPM and the time at which the gel becomes a liquid and flows from the top of the vial is taken as the degelling time (supplementary information, Figure S1).

The gel strength can be more precisely examined using rheology, where the strength of the gel is determined from the flat plateau of the storage modulus (G') (Figure 4). A higher G'value in the plateau region indicates a stronger gel. As the amount of ODA in the sample was increased from 10 mg/mL to 50 mg/mL, there was first an increase in the gel strength followed by a decrease at 50 mg/mL. From 10 mg/mL to 40 mg/mL the increase in gel strength is as expected due to the increase in the amount of crosslinking agent, ODA, which leads to additional physical associations between nanocellulose particles. The ODA adsorbs at one end onto the nanocellulose surface through interactions of the ODA amine groups with the O-CNC carboxyl groups. The ODA hydrocarbon tails interact via solvophobic interactions and drive formation of a stiff gel. At the highest ODA concentration, the gel strength decreases, likely due to undissolved, aggregated ODA disrupting the network. These rheological tests provide a precise view of the gel strength and differentiation between the different samples and the results are consistent with the simple shaking tests (supplementary information, Figure S1). While there is a significant difference when increasing from 10 mg/mL ODA to 30 mg/mL ODA, the additional strength when increasing to 40 mg/mL is very minimal, so we select a ratio of 3:1 ODA:O-CNC by weight (10 mg/mL O-CNC and 30 mg/mL ODA)) as the optimal ratio for the gels.

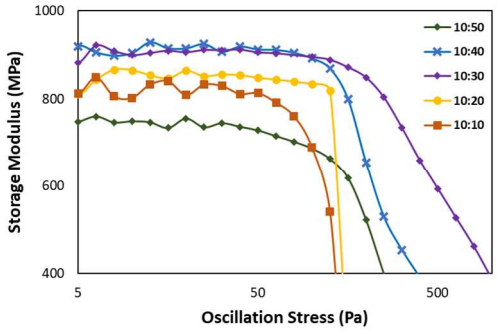

Figure 4: Storage modulus as a function of oscillation stress for nanocellulose organogels with increasing concentrations of ODA and 10 mg/mL of O-CNC (O-CNC:ODA mg/mL in legend)

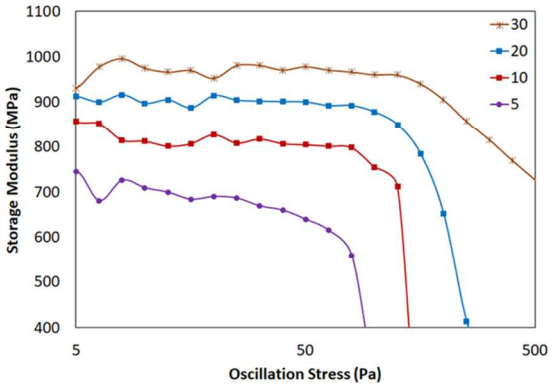

Figure 5: Storage modulus as a function of oscillation stress for increasing O-CNC concentration and constant ODA to O-CNC ratio of 3:1. (Amount of O-CNC in mg/mL is indicated in the legend).

In addition to the ratio of ODA to O-CNC and amount of ODA in the gels, the concentration of O-CNCs dispersed in DMSO influences the gel strength (Figure 5). At low concentrations of O-CNC, the gels are weak and they strengthen at higher O-CNC concentrations. A maximum dispersion of O-CNC in DMSO is observed around 50 mg/mL, at which point the O-CNCs aggregate and settle and are no longer part of the suspension where gelation occurs. While keeping a 3:1 ratio of ODA to O-CNC, identified as sufficient for gelation as discussed above, the amount of O-CNC was increased and an increase in gel strength was seen until 30 mg/mL O-CNC (Figure 5). Upon shaking gels with these same concentrations, a similar pattern was observed (supplementary information, Figure S2).

The degree of oxidation of the nanocellulose was also found to be an important factor in the strength of the gels. This is due to the number of carboxylate groups that are available for network formation as the ODA is added. Only shaking tests were performed to compare the degree of oxidation since these provided sufficiently consistent data and agreement with the rheological studies. At a low degree of oxidation (0.15), the gelation was disrupted three times earlier upon shaking than with a degree of oxidation of 0.30 (supplementary information, Figures S3 and S4). While all the gels made with O-CNC with a degree of oxidation of 0.15 degelled by 4 min, the gels containing O-CNC with a degree of oxidation of 0.30 remained gelled for up to 15 min for the 3:1 ratio.

The complexity of the multicomponent system means that the order of mixing may also be important to gel formation. There are three potential methods: 1) dispersion of O-

CNCs in DMSO followed by addition of ODA powder, 2) dissolution of ODA in DMSO followed by addition of O-CNC powder, and 3) dissolution of ODA in DMSO and dispersion of O-CNC in DMSO followed by mixing of the two solutions. Due to ODA's low solubility in room temperature DMSO, it is difficult to dissolve after O-CNCs are in solution, so method (1) resulted in insoluble ODA and poor gels. O-CNCs disperse well in DMSO whether ODA is present or not, so method (2) produced good gels. This method also enabled ODA to interact with the O-CNCs as they were being wet by the DMSO, increasing the area of interaction and improving gel strength. Method (3) showed similar results to (2), so method (2) was chosen as the main mixing technique.

Finally, the gel formation is also sensitive to heating and cooling conditions. For all samples, the mixtures were heated to 70°C to disrupt the initial hydrogen bonds and promote homogeneous mixing. They were vortexed for 15 sec and then subjected to cooling to room temperature or below. Rapid cooling via quenching in an ice bath, did not result in formation of strong gels. This is because the structure was frozen into place without leaving flexibility for the ODA chains to arrange and form networks. The freezing point of DMSO is 19°C, so cooling to ice bath temperatures freezes the entire structure. A slower cool to 4°C in a refrigerator produces strong gels that remain gelled at room temperature. Though this also results in frozen DMSO during gelling, the speed of cooling is slower and ODA is able to rearrange and form networks prior to DMSO freezing. While it avoids the DMSO freezing complication, cooling directly to room temperature is too slow and results in aggregation of O-CNCs and settling of the particle aggregates. In comparing the 3:1 ODA:O-CNC for each of the three cooling procedures, the slow cooled gel degelled the fastest at 2 min followed by the quenched gel at 10 min, and the refrigerated gel stayed gelled the longest and was disrupted after 15 min of shaking. The gel formation, though enhanced by DMSO freezing, is not solely caused by the freezing of the solvent. Gel formation did not occur for O-CNC without ODA or for O-CNC with other amines, such as diaminooctane and polyethyleneimine (supplementary information, Figures S5 and S6). The DMSO acts as a gelation promotor for the O-CNC/ODA network, but is not the sole contributor to gel formation. Thus, cooling slowly to 4□ is the optimal process for forming O-CNC gels in DMSO.

Following these studies on nanocellulose organogel formation, we determined that a standard gel system with a degree of oxidation of 0.30, 10 mg/mL O-CNC, 30 mg/mL ODA, a mixing order of dissolution of ODA in DMSO followed by addition of O-CNC powder and slow cooling to 4□ is an appropriate starting system for incorporation of APIs into the gels.

Incorporation of APIs into nanocellulose gels

APIs, in concentrations ranging from 50-500 mg/mL, were incorporated into the nanocellulose organogels by dissolving them

in the DMSO, O-CNC, and ODA mixture, heating to 70□ to thoroughly mix the materials, and cooling via the same procedure as for the nanocellulose gels without APIs. The gels were then returned to room temperature for observation. The APIs incorporated into the nanocellulose gels were dried and characterized using DSC and XRD.

When APIs are incorporated into the gels, they show diverse effects on the gel strength (Figure 6). Rheological studies of API loaded gels indicate that inclusion of API disrupts network formation and decreases the gel strength as seen by a decrease in the storage moduli in the plateau region for SP (yellow triangles) and SMX (green diamonds) in comparison to the gel without any loaded drug (purple circles). This weakening of the gel was also observed in shaking tests performed on the API incorporated gels (supplementary information, Figure S7), where SP degels the fastest at 2 min and SMX behaves similarly to the drug free gels, breaking after 10 min of shaking. This is likely due to API crystals collecting in the solvophobic chains of the ODA, causing a disruption in the network. For the case of SMX, as higher amounts of API were added, the degelation time in the shaking tests was also faster (supplementary information, Figure S8), which is not the case for the drug-free gels, indicating that, similar to SP, SMX also disrupts the gel network, but requires higher concentrations. The SMZ, however, strengthens the network (Figure 6, blue squares) and the gel does not break until 20 min of shaking (supplementary information, Figure S7-D, H). This is likely due to favorable interactions between the drug and the cross-linker molecules of ODA, resulting in a stiffer gel.

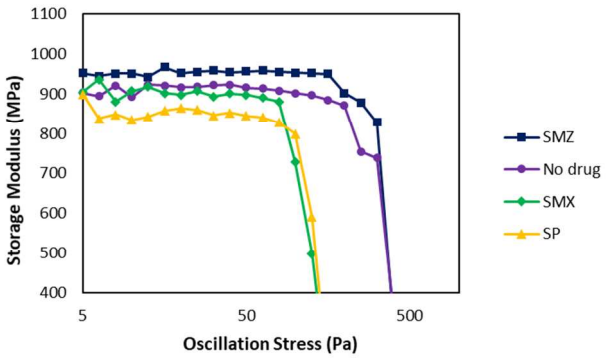

Figure 6: Storage modulus as a function of oscillation stress of gels containing 10 mg/mL O-CNC, 30 mg/mL ODA, and 200 mg/mL of SMZ (blue squares), SMX (green diamonds), and SP (yellow triangles). Purple contains no API.

Sulfamethoxazole (SMX) solid form

The as-received SMX showed a melting peak onset at 168□, in agreement with the literature of SMX form I and IV, which melt at 170□ (Figure 7).[32] There is an exotherm observed starting at 230□ with a peak at 273□ for as-received SMX, which arises due to the oxidation of the byproducts resulting from heating SMX. This was confirmed using thermal gravimetric analysis (TGA) (supplementary information, Figure S9).[56] SMX recovered from the dried gel did not show a melting peak, indicating that the API in the gel was not in a crystalline form (Figure 7, blue curve). There is a small endotherm at 55□, which corresponds to melting of the ODA. The

degradation exotherm of the SMX at 272□ is still present, however, indicating that the API is still present in the material, likely in its amorphous form. The only other component within the gels is the O-CNC, which shows decomposition peaks between 220 and 280□ that are insignificant compared to those from the SMX.

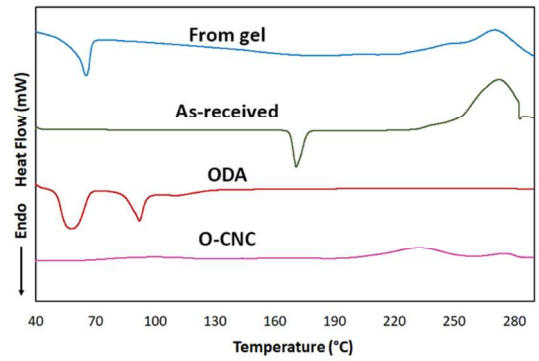

Figure 7: DSC thermograms of dried gels prepared from SMX (blue), as-received SMX (green), ODA (red) and O-CNCs (pink)

XRD was performed on each individual component of the gel, the commercially available APIs, as well as on the dried gels to determine the crystal structure of each and note any major changes in the crystal structure of the API polymorphs and the resulting powder patterns are shown in Figure 8. The XRD data for the dried gel was missing a bulk of the major peaks seen on the as-received SMX, especially obvious between 9° and 21°. Peaks were seen from ODA at 21.9° and O-CNC at 27.7° and 32° and only minor peaks were seen outside of those regions, indicating that the API was primarily amorphous in the dried gel. The recovered API powder pattern was further analyzed against the simulated XRD powder patterns available for all the different polymorphs of the SMX, obtained from the Cambridge Crystallography Data Centre (CCDC) (supplementary information, Figure S10). In comparing the other polymorphs to the dried gel containing SMX, none of them showed significant similarities to the minor peaks at low 2-theta for the SMX in the gels (Figure 8, blue curve), further indicating that the API within the gel was primarily amorphous.

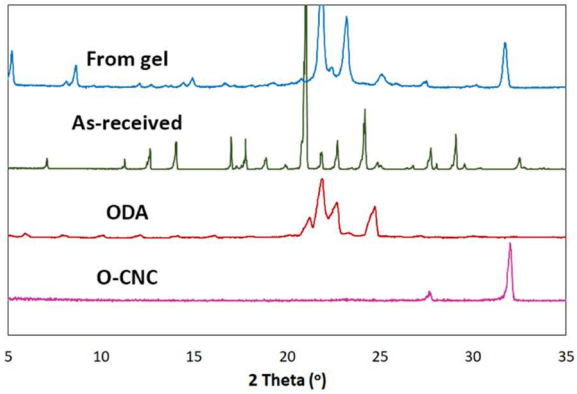

Figure 8: XRD powder patterns of dried gels prepared from SMX (blue), as-received SMX (green), ODA (red) and O-CNCs (pink)

The SMX obtained from the gel was also compared with SMX crystallized from DMSO as well as SMX crystallized from an ODA-DMSO mixture. SMX forms a solvate with DMSO as noted by the appearance of a peak in the DSC (supplementary information, Figure S11) at 104□, relating to the desolvation temperature. A melting peak is no longer observed since the solvate starts degrading immediately after, as seen in the TGA curve (supplementary information, Figure S9) where mass loss is

seen starting at 106.5□. The SMX obtained from the ODA-DMSO mixture does not show a distinct melting peak. Instead, there is a broad peak, which could be due to some interactions between the ODA and the SMX. The XRD patterns for these (supplementary information, Figure S12) show a number of peaks for both of these SMX samples. The peaks from these line up very closely, indicating that the SMX from the ODA-DMSO mixture and the SMX from DMSO are both similar in crystal structure. Importantly, the form of the SMX crystallized in DMSO and ODA-DMSO is different from that crystallized from the nanocellulose gels, which was primarily amorphous.

Sulfapyridine (SP) solid form

SP was similarly added to the organogels in concentrations ranging from 50 mg/mL to 300 mg/mL. The recovered SP from the dried gel showed a similar melting temperature to the as-received with an onset for the melting peak at 186□ (Figure 9).

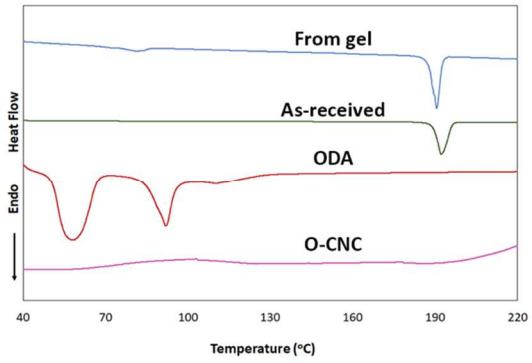

Figure 9: DSC thermograms of dried gels prepared from SP (blue), as-received SP (green), ODA (red) and O-CNCs (pink)

There is a second small endotherm in the API recovered from the gel at 80□, but this is attributed to the ODA since there is a mixture of ODA, O-CNC, and SP present upon drying. This melting temperature points to the API being in form I, which is the stable polymorph at room temperature. It has been noted that most other forms (II, III, IV, and V) all slowly change to phase I when left at room temperature. The melting points for the other forms are 181□, 179□, 174□, 176□ and 167□ for forms II, III, and IV, V, and VI respectively. [50,57,58] Many of these are so close that it is difficult to distinguish, so further analysis via XRD was critical.

XRD analysis for SP does not fully agree with the observation that the polymorph is the same as as-received, form I. The recovered SP in the dried gel is compared to the as-received SP in Figure 10. The peaks present in the as-received SP, which correspond to form I based on DSC analysis, are also present in the dried gel, as are the peaks corresponding to ODA and O-CNC. However, there are significantly more peaks than can be accounted for by these three controls. The powder pattern for the SP from the dried gel was also compared to the powder XRD patterns of the various forms of SP obtained from the CCDC and it was noted that the product was in fact a combination of the various polymorphs (supplementary information, Figure S13). The recovered API appears to be a mixture of polymorphs I, III and V since most of the peaks line up with these forms. By performing crystallization in a confined gel with sites for heterogeneous nucleation, we

get a mixture of polymorphs, rather than only the most stable polymorph I. Further refinement of the nanocellulose surface and gel environment may allow more precise tuning of the polymorph.

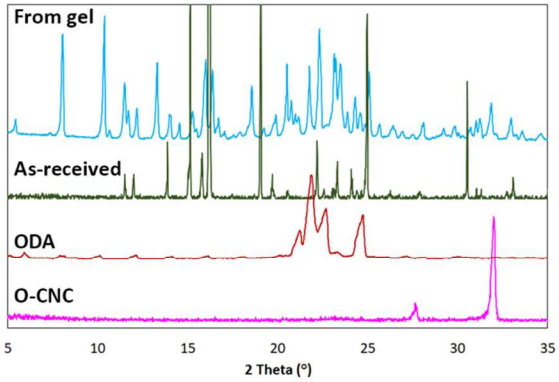

Figure 10: XRD powder patterns of dried gels prepared from SP (blue), as-received SP (green), ODA (red) and O-CNCs (pink)

SP was also crystallized out of DMSO and an ODA-DMSO mixture. Out of DMSO, SP was obtained as a solvate with an onset for the desolvation peak at 98.7□ (supplementary information, Figure S14). The sample starts to degrade after desolvation at 100.4□, as observed in the TGA analysis (supplementary information, Figure S15) and therefore does not show a melting peak. The melting peak of the SP from the ODA-DMSO mixture has an onset at 181.6□, which is close to the temperatures for the as-received SP. The XRD data for these SP samples are shown in supplementary information, Figures S13 and S16. From the powder patterns, we see that the SP crystallized from DMSO solvate is most closely related to polymorph II and shows some similarities to the as-received SP, while the SP from the ODA-DMSO mixture is mostly polymorph III. As with the SMX, neither of these are the same mixture of forms as the SP crystallized from the gel.

Sulfamerazine (SMZ) solid form

SMZ was added to the organogels during the network formation step. The DSC thermogram of the as-received SMZ from Alfa Aesar (Figure 11, green curve) showed a melting peak at 234□, which is attributed to polymorph I of SMZ, which has a melting peak at 237□.[59] The recovered SMZ in the dried gel showed two peaks, one from the ODA melting at 83□ and another melting peak at 226□, which could be from the melting of a mixture of polymorphs I and II of SMZ (Figure 11, blue curve), as form II is known to melt at 228°C. [51,59] Form II has a tendency to transform to form I on heating, which typically presents as an endotherm with an onset at between 160-180□,[51,59,60] and is missing from both the as-received and the recovered SMZ. This could indicate the existence of polymorph II in a stable form at higher temperatures. Due to the melting points being close together, further analysis is necessary using XRD powder patterns.

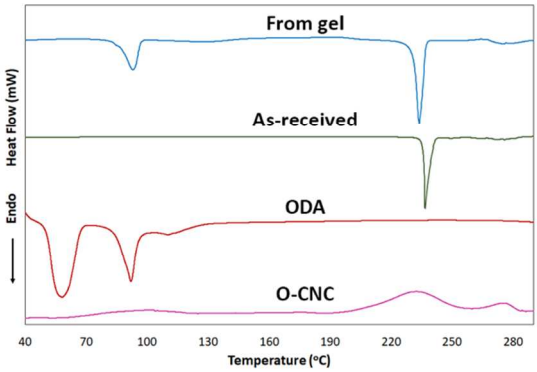

Figure 11: DSC thermograms of dried gels prepared from SMZ (blue), as-received SMZ (green), ODA (red) and O-CNCs (pink)

The as-received SMZ was confirmed to be polymorph I using the powder patterns (supplementary information, Figure S17). The recovered SMZ from the gel, however, did not fully match the powder pattern for the as-received SMZ (Figure 12). It, instead, appears to be a combination of multiple polymorphs. Strong peaks at approximately 15.5° and 19° correspond to polymorph II and are not present in the as-received material, while a strong peak at approximately 14.8° corresponds to polymorph I and is also present in the as-received material. Interestingly, the strong peak at approximately 19.5° is only predicted to occur for form P $2_1/c$ and is also clearly present in the dried gel containing SMZ. We did not analyze the API peaks in the region of 20-25° due to significant overlap with the ODA peaks. From these results, we can conclude that the SMZ in the dried gel is not uniformly the same polymorph as the starting material, and instead is a mixture of multiple polymorphs, including polymorph I and II and potentially also P $2_1/c$.

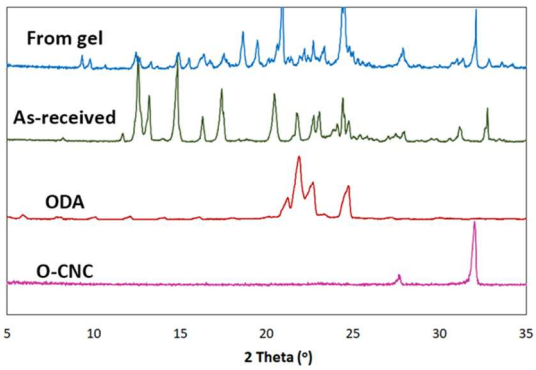

Figure 12: XRD powder patterns of SMZ prepared from dried gel (blue), as-received SMZ (green), ODA (red) and O-CNCs (pink)

SMZ was also crystallized from DMSO and a mixture of ODA and DMSO. DSC thermograms (supplementary information, Figure S18) show that SMZ from DMSO has a melting peak with an onset temperature of 228.2□. Though this is slightly lower than the onset for the as-received SMZ, the XRD powder pattern (supplementary information, Figure S19) matches the as-received almost exactly, indicating that the DMSO-crystallized SMZ is the same polymorph as the as-received SMZ. XRD data shows that the SMZ obtained from the ODA-DMSO mixture was in almost the same crystal structure as SMZ from the gel. The DSC showed that the onset temperature for the melting peak of this SMZ sample was at 227.8□. This sample also did not show any polymorph transition peaks, indicating that it was very similar to the SMZ from the gel. While the polymorph was similar, the shape of the crystals showed distinct differences. SMZ from the ODA-DMSO mixture nucleated as needle-shaped crystals ranging between 30-100 μm in size (Figure 13-A). The SMZ crystallized from the gel had a much lower aspect ratio (Figure 13-B), potentially due to confinement effects from crystallization within the gel.

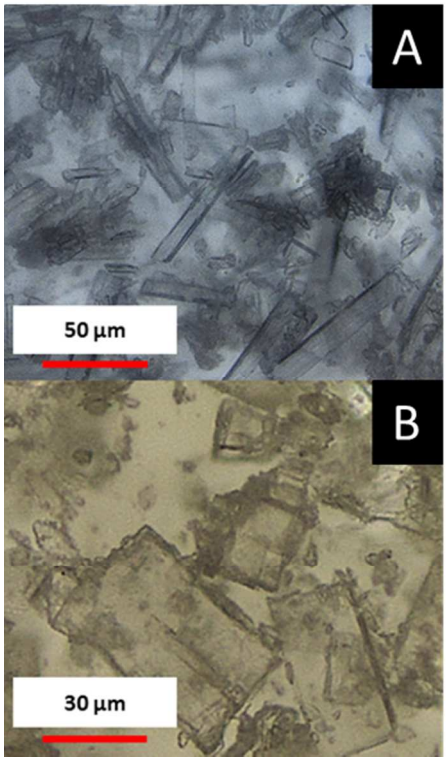

Figure 13: Optical microscopy images of A SMZ crystallized from the dried ODA-DMSO mixture, and B SMZ crystals recovered from the dried gel

Dissolution testing

Dissolution testing was performed on the gels prepared in this work for SMX, SP and SMZ and the dissolution rates and extent of dissolution were compared to as-received powder and a physical mixture of API, O-CNCs and ODA (Figure 14). Since the API form is different in the gels than the as-received powder, the dissolution rates are expected to be different, particularly for SMX, which is in the amorphous form, known to be less thermodynamically stable. For SMX, the dissolution rate for the drug from the gels is more gradual but ultimately ends up at the same amount as the as-received API and the physical mixture (Figure 14-A). This points to a sustained release of the recovered API, likely due to particle stabilization by the ODA molecules. In water, ODA acts as a surfactant, adsorbing to the surface of the API particles and stabilizing their dispersion in water, slowing down dissolution.[61-63] For SP, the maximum amount dissolved for the API recovered from the gel was much lower than the as-received and the physical mixture (Figure 14-B). This indicates that ODA interacts more strongly with the SP molecules causing a higher level of physical entrapment and reducing the overall dissolution. This result correlates with the decrease in the gel network strength when SP is incorporated into the system (Figure 6), as the ODA closely interacts with the SP and the O-CNCs no longer remain cross-linked. The SMZ release initially occurs as a small burst but then slows down and is much more gradual between 100-600 min. It reaches the same level of dissolution as the as-received and the physical mixture but takes almost double the amount of time. This is again likely due to entrapment by the ODA causing a slowing down of the drug dissolution in HCl.[63,64] Extended release of this sort presents several advantages for certain applications such as increased drug residence within the body, allowing for increased uptake and increased stability.[4] The difference between the physical mixture and gels is likely due to the ODA being in intimate contact with the API in the gels, as opposed to present as large particles that must first themselves dissolve in water before it can act as a surfactant for the physical mixture.

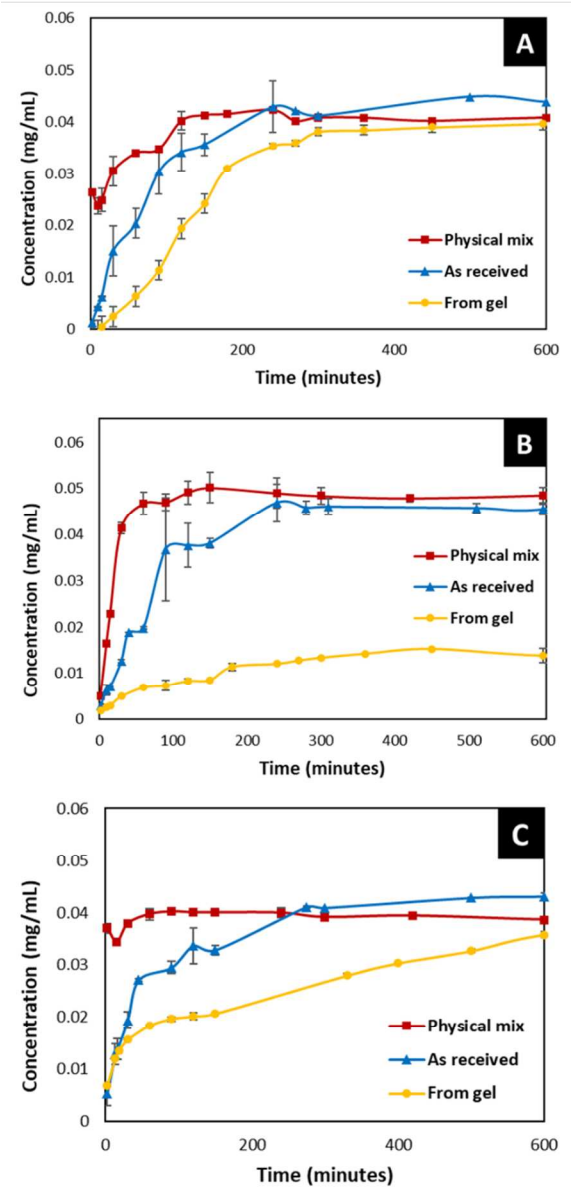

Figure 14: Dissolution of A) SMX, B) SP, C) SMZ from physical mixtures (red squares), as received powder (blue triangles), and drug recovered from gel (yellow circles). Error bars were obtained from the standard deviation of 3 trials.

Discussion

In this work, we have shown that organogels based on surface modified nanocellulose can be utilized to promote crystallization of APIs in different polymorphs than the most stable or to prevent crystallization. Nanocellulose modified through oxidation can be further mixed with gelation agents, such as ODA, to develop organogels by creating physical networks in organic solvents. This is a relatively new development in nanocellulosic materials, as a majority of studies on gels are focused on hydrogels. Here, we focused on oxidizing nanocellulose and using an amine-based surfactant as the gelation agent to perform crystallization in DMSO. The optimization of the O-CNC/ODA organogels was done by tuning several contributing factors, including changing the concentrations of O-CNC and ODA, changing the ratio of ODA to O-CNC, and varying the mixing and cooling conditions for the gels. Optimized conditions for gel formation were found to be a degree of oxidation of 0.30, 10 mg/mL O-CNC, 30 mg/mL ODA, a mixing order of dissolution of ODA in DMSO followed by addition of O-CNC powder and slow cooling to 4□. Though the focus was on this particular material system, the nanocellulose surface can be modified using many other functional groups and one can build upon these results to design a platform for organogel formation in a variety of solvents and with many different functionalities.

APIs are introduced into the gel components prior to heating and cooling for gel formation, and they are expected to incorporate into the solvophobic part of the network. Upon recovery from the gels, it

was seen that SMX was produced in an amorphous form. SP, which was received in form I, was crystallized as a mixture of forms I, III and V, and SMZ was received as form I but recovered as a mixture of polymorph I and II and potentially some transitions to form P $2_1/c$. The API polymorphs from the gels are also different than those of the drugs crystallized from DMSO and a mixture of ODA-DMSO for SMX and SP, while, though the same polymorph, the crystal shape is different for SMZ. This indicates that the gel phase recrystallization has a significant effect on the structure of the recovered APIs. An interesting observation from this study is the occurrence of polymorph mixtures for the two APIs that crystallized in the gels. This indicates the presence of multiple crystallization environments for the different polymorphs to form, which could be homogeneous crystallization in the bulk and heterogeneous crystallization in the gels or different regions in the gels themselves. As nanocellulose is a natural material extracted from wood sources, heterogeneities are common and these could be contributing to the formation of different zones in the gels. Further in-depth analysis of nanocellulose sources will provide greater insight into this phenomenon.

Dissolution testing illuminated the success in developing a sustained release system for two of the APIs, SMX and SMZ. It was found that these APIs from the gels dissolved more slowly but reached the same overall dissolution amount. This is likely due to the presence of well-dispersed ODA, which acts as a surfactant that can stabilize the highly hydrophobic API particles. This nanocellulose organogel system can thus be used to control the release of APIs to create a more uniform dissolution profile, resulting in a higher overall absorption of the drug. For SP, dissolution testing presented a challenge in the selection of gelation or crosslinking agents since SP dissolved to a lesser extent than the as-received powder and a physical mixture of API, O-CNC and ODA. Selection of crosslinking agents thus appears to be an important parameter for moving forward with these materials for drug delivery applications, and approaches such as chemically attaching the crosslinking agent to the nanocellulose will be explored to overcome this limitation.

Conclusions

This study showed that it is possible to shift the polymorph of pharmaceutical crystals through crystallization in a surface-modified nanocellulose gel. This is a particularly exciting demonstration of using natural materials that are readily surface modified to form a tailored environment for drug crystallization. Building off this platform, the nanocellulose surface and gelation agents can be rationally designed to provide environments to specifically drive formation of chosen polymorphs in a variety of organic solvents. This provides a promising first step in a new technology for pharmaceutical crystal engineering and production of dosage forms with more sustained release profiles.

Conflicts of Interest

There are no conflicts of interest to declare.

Acknowledgements

MB was supported by the Renewable Bioproducts Institute at Georgia Tech, SS was supported by the Presidents Undergraduate Research Award at Georgia Tech, and HW was supported by Grant HDTRA11810004. This work was performed in part at the Georgia Tech Institute for Electronics and Nanotechnology, a member of the National Nanotechnology Coordinated Infrastructure, which is supported by the National Science Foundation (Grant ECCS-1542174). Work was also performed in the Center for the Science and Technology for Advanced Materials and Interfaces Polymer Characterization Lab and Natalie Stingelin's lab at Georgia Tech.

References

1 S. L. Childs, P. Kandi and S. R. Lingireddy, *Mol. Pharmaceutics*, 2013, **10**, 3112–3127.

2 S. Kalepu and V. Nekkanti, *Acta Pharmaceutica Sinica B*, 2015, **5**, 442–453.

3 S. M. Guthrie, D.-M. Smilgies and G. Giri, *Crystal Growth & Design*, 2018, **18**, 602–606.

4 C. Loira-Pastoriza, J. Todoroff and R. Vanbever, *Advanced Drug Delivery Reviews*, 2014, **75**, 81–91.

5 P. Augustijns and M. E. Brewster, *Journal of Pharmaceutical Sciences*, 2012, **101**, 7–9.

6 J. S. LaFountaine, L. K. Prasad, D. A. Miller, J. W. McGinity and R. O. Williams III, *European Journal of Pharmaceutics and Biopharmaceutics*, 2017, **113**, 157–167.

7 G. Agarwal, S. Agarwal, P. K. Karar and S. Goyal, *American Journal of Advanced Drug Delivery*, 2017, **5**, 64–76.

8 E. D. Schoenberg, D. A. Blake, F. B. Swann, A. W. Parlin, D. Zurakowski, C. E. Margo, T. Ponnusamy, V. T. John and R. S. Ayyala, *Trans. Vis. Sci. Tech.*, 2015, **4**, 4–9.

9 B. C. Hancock and M. Parks, *Pharm Res*, 2000, **17**, 397–404.

10 G. T. Rengarajan, D. Enke, M. Steinhart and M. Beiner, *J. Mater. Chem.*, 2008, **18**, 2537–3.

11 M. E. Matteucci, B. K. Brettmann, T. L. Rogers, E. J. Elder, R. O. Williams and K. P. Johnston, *Mol. Pharmaceutics*, 2007, **4**, 782–793.

12 J. M. Ting, W. W. Porter III, J. M. Mecca, F. S. Bates and T. M. Reineke, *Bioconjugate Chem.*, 2018, **29**, 939–952.

13 A. L. Sarode, H. Sandhu, N. Shah, W. Malick and H. Zia, *Mol. Pharmaceutics*, 2013, **10**, 3665–3675.

14 A. M. Agrawal, M. S. Dudhedia and E. Zimny, *AAPS PharmSciTech*, 2015, **17**, 133–147.

15 B. Brettmann, E. Bell, A. Myerson and B. L. Trout, *Journal of Pharmaceutical Sciences*, 2012, **101**, 1538–1545.

16 B. K. Brettmann, A. S. Myerson and B. Trout, *Journal of Pharmaceutical Sciences*, 2012, **101**, 2185–2193.

17 J. Sun, F. Wang, Y. Sui, Z. She, W. Zhai, C. Wang and Y. Deng, *IJN*, 2012, 5733–12.

18 N. J. Babu and A. Nangia, *Crystal Growth & Design*, 2011, **11**, 2662–2679.

19 H. Kempe, A. Parareda Pujolràs and M. Kempe, *Pharm Res*, 2014, **32**, 375–388.

20 R. Hiremath, J. A. Basile, S. W. Varney and J. A. Swift, *J. Am. Chem. Soc.*, 2005, **127**, 18321–18327.

21 L. J. Chyall, J. M. Tower, D. A. Coates,

T. L. Houston and S. L. Childs, *Crystal Growth & Design*, 2002, **2**, 505–510.
22 J.-M. Ha, J. H. Wolf, M. A. Hillmyer and M. D. Ward, *J. Am. Chem. Soc.*, 2004, **126**, 3382–3383.
23 J. Ling and K. Chadwick, *Org. Process Res. Dev.*, 2017, **21**, 827–834.
24 M. Lang, A. L. Grzesiak and A. J. Matzger, *J. Am. Chem. Soc.*, 2002, **124**, 14834–14835.
25 J. L. Quon, K. Chadwick, G. P. F. Wood, I. Sheu, B. K. Brettmann, A. S. Myerson and B. L. Trout, *Langmuir*, 2013, **29**, 3292–3300.
26 H. B. Eral, V. López-Mejías, M. O'Mahony, B. L. Trout, A. S. Myerson and P. S. Doyle, *Crystal Growth & Design*, 2014, **14**, 2073–2082.
27 Y. Diao, M. E. Helgeson, A. S. Myerson, T. A. Hatton, P. S. Doyle and B. L. Trout, *J. Am. Chem. Soc.*, 2011, **133**, 3756–3759.
28 Y. Diao, A. S. Myerson, T. A. Hatton and B. L. Trout, *Langmuir*, 2011, **27**, 5324–5334.
29 S. Ueno, Y. Hamada and K. Sato, *Crystal Growth & Design*, 2003, **3**, 935–939.
30 P. W. Carter and M. D. Ward, *J. Am. Chem. Soc.*, 1994, **116**, 769–770.
31 R. Hiremath, S. W. Varney and J. A. Swift, *Chemical Communications*, 2004, 2676–2.
32 C. P. Price, A. L. Grzesiak and A. J. Matzger, *J. Am. Chem. Soc.*, 2005, **127**, 5512–5517.
33 A. Y. Lee, I. S. Lee, S. S. Dette, J. Boerner and A. S. Myerson, *J. Am. Chem. Soc.*, 2005, **127**, 14982–14983.
34 A. J. Page and R. P. Sear, *Physical Review Letters*, 2006, **97**, 065701–4.
35 Y. Diao, M. E. Helgeson, Z. A. Siam, P. S. Doyle, A. S. Myerson, T. A. Hatton and B. L. Trout, *Crystal Growth & Design*, 2011, **12**, 508–517.
36 L. Kaufmann, S. R. Kennedy, C. D. Jones and J. W. Steed, *Chemical Communications*, 2016, **52**, 10113–10116.
37 F. Aparicio, E. Matesanz and L. Sánchez, *Chemical Communications*, 2012, **48**, 5757–3.
38 J. A. Foster, M.-O. M. Piepenbrock, G. O. Lloyd, N. Clarke, J. A. K. Howard and J. W. Steed, *Nature Chem*, 2010, **2**, 1037–1043.
39 J. A. Foster, K. K. Damodaran, A. Maurin, G. M. Day, H. P. G. Thompson, G. J. Cameron, J. C. Bernal and J. W. Steed, *Chemical Science*, 2016, **8**, 78–84.
40 R. J. Moon, A. Martini, J. Nairn, J. Simonsen and J. Youngblood, *Chemical Society Reviews*, 2011, **40**, 3941–54.
41 M. S. Reid, M. Villalobos and E. D. Cranston, *Langmuir*, 2017, **33**, 1583–1598.
42 S. Shafiei-Sabet, W. Y. Hamad and S. G. Hatzikiriakos, *Langmuir*, 2012, **28**, 17124–17133.
43 L. Lewis, M. Derakhshandeh, S. G. Hatzikiriakos, W. Y. Hamad and M. J. MacLachlan, *Biomacromolecules*, 2016, **17**, 2747–2754.
44 L. Heath and W. Thielemans, *Green Chem.*, 2010, **12**, 1448–6.
45 H. Valo, S. Arola, P. Laaksonen, M. Torkkeli, L. Peltonen, M. B. Linder, R. Serimaa, S. Kuga, J. Hirvonen and T. Laaksonen, *European Journal of Pharmaceutical Sciences*, 2013, **50**, 69–77.
46 L. Huang, X. Chen, T. X. Nguyen, H. Tang, L. Zhang and G. Yang, *J. Mater. Chem. B*, 2013, **1**, 2976–9.
47 R. Kolakovic, L. Peltonen, A. Laukkanen, J. Hirvonen and T. Laaksonen, *European Journal of Pharmaceutics and Biopharmaceutics*, 2012, **82**, 308–315.
48 M. Badshah, H. Ullah, S. A. Khan, J.

K. Park and T. Khan, *Cellulose*, 2017, 1–12.
49 C. Ruiz-Palomero, S. R. Kennedy, M. L. Soriano, C. D. Jones, M. V. X. rcel and J. W. Steed, *Chemical Communications*, 2016, **52**, 7782–7785.
50 A. Burger, K. Schulte and R. Ramberger, *Journal of Thermal Analysis*, 1980, **19**, 475–484.
51 G. G. Z. Zhang, C. Gu, M. T. Zell, R. T. Burkhardt, E. J. Munson and D. J. W. Grant, *Journal of Pharmaceutical Sciences*, 2002, **91**, 1089–1100.
52 Y. Habibi, H. Chanzy and M. R. Vignon, *Cellulose*, 2006, **13**, 679–687.
53 J. Araki, M. Wada and S. Kuga, *Langmuir*, 2001, **17**, 21–27.
54 D. da Silva Perez, S. Montanari and M. R. Vignon, *Biomacromolecules*, 2003, **4**, 1417–1425.
55 S. R. Raghavan and B. H. Cipriano, in *Molecular Gels Materials with Self-Assembled Fibrillar Network*, eds. R. G. Weiss and P. Terech, 2005, pp. 233–244.
56 N. S. Fernandes, M. A. D. S. Carvalho Filho, R. A. Mendes and M. Ionashiro, *Journal of the Brazilian Chemical Society*, 1999, **10**, 459–462.
57 A. Burger and R. Ramberger, *Mikrochimica Acta*, 1979, **72**, 273–316.
58 R. N. Castle and N. F. Witt, *J. Am. Chem. Soc.*, 1946, **68**, 64–66.
59 M. R. Caria and R. Mohamed, *Acta Cryst (1992). B48, 492-498 [doi:10.1107/S0108768192000910]*, 1992, 1–7.
60 K. Kawakami, Y. Asami and I. Takenoshita, *Journal of Pharmaceutical Sciences*, 2010, **99**, 76–81.
61 P. Knöös, S. Onder, L. Pedersen, L. Piculell, S. Ulvenlund and M. Wahlgren, *Elsevier*, 2013, **3**, 7–14.
62 G. Blume and G. Cevc, *Biochimica et Biophysica Acta (BBA) - Biomembranes*, 1990, **1029**, 91–97.
63 M. N. Sahib, Y. Darwis, K. K. Peh, S. A. Abdulameer and Y. T. Fung Tan, *Drug Dev. Res.*, 2012, **73**, 90–105.
64 D. Marsh, R. Bartucci and L. Sportelli, *Biochimica et Biophysica Acta (BBA) - Biomembranes*, 2003, **1615**, 33–59.

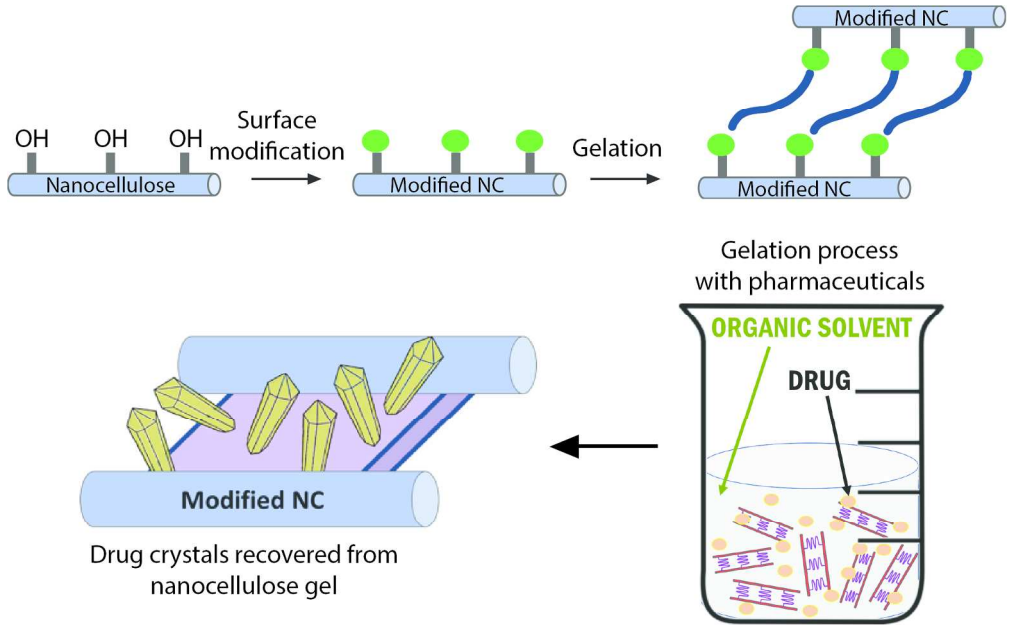

191x118mm (300 x 300 DPI)